

Local inspection of magnetic properties in GdMnIn by measuring hyperfine interactions

Cite as: AIP Advances 11, 015322 (2021); <https://doi.org/10.1063/9.0000037>

Submitted: 10 October 2020 . Accepted: 12 December 2020 . Published Online: 08 January 2021

G. A. Cabrera-Pasca, J. F. Magno, W. L. Ferreira, A. C. Campos, B. Bosch-Santos, T. S. N. Sales, L. F. D. Pereira,  A. Burimova,  R. N. Saxena,  R. S. Freitas, and  A. W. Carbonari

COLLECTIONS

Paper published as part of the special topic on [65th Annual Conference on Magnetism and Magnetic MaterialsMMM2021](#)



View Online



Export Citation



CrossMark

ARTICLES YOU MAY BE INTERESTED IN

[S is for Science: The making of 3-2-1 Contact](#)

Physics Today **74**, 26 (2021); <https://doi.org/10.1063/PT.3.4654>

[Sildenafil tablet analyzed by XPS](#)

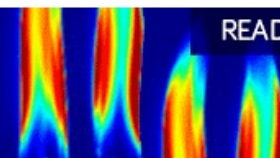
Surface Science Spectra **27**, 024016 (2020); <https://doi.org/10.1116/6.0000609>

[Practical guides for x-ray photoelectron spectroscopy \(XPS\): Interpreting the carbon 1s spectrum](#)

Journal of Vacuum Science & Technology A **39**, 013204 (2021); <https://doi.org/10.1116/6.0000682>

AIP Advances
Fluids and Plasmas Collection

READ NOW





Local inspection of magnetic properties in GdMnIn by measuring hyperfine interactions

Cite as: AIP Advances 11, 015322 (2021); doi: 10.1063/9.0000037

Presented: 2 November 2020 • Submitted: 10 October 2020 •

Accepted: 12 December 2020 • Published Online: 8 January 2021



G. A. Cabrera-Pasca,¹ J. F. Magno,¹ W. L. Ferreira,² A. C. Campos,² B. Bosch-Santos,² T. S. N. Sales,² L. F. D. Pereira,² A. Burimova,²  R. N. Saxena,²  R. S. Freitas,³  and A. W. Carbonari^{2,a)} 

AFFILIATIONS

¹Faculdade de Ciências Exatas e Tecnologia, Universidade Federal do Pará, 68440-000 Abaetetuba, PA, Brazil

²Instituto de Pesquisas Energéticas e Nucleares, IPEN-CNEN/SP, University of São Paulo, 05508-000 São Paulo, SP, Brazil

³Instituto de Física, Universidade de São Paulo, 05508-090 São Paulo, SP, Brazil

Note: This paper was presented at the 65th Annual Conference on Magnetism and Magnetic Materials.

a) Author to whom correspondence should be addressed: carbonar@ipen.br

ABSTRACT

GdMnIn is reported to crystallize in the hexagonal MgNi₂-type structure presenting a spin-glass behavior with no magnetic order attributed to the triangular spin frustration of magnetic ions. In the present work, FC-ZFC magnetization, specific heat and AC susceptibility measurements along with the local magnetic exchange measured by hyperfine interactions at In sites are used to investigate the magnetic behavior in GdMnIn compound. The ZFC-FC magnetization curves exhibit an inflection which was ascribed to the antiferromagnetic transition at $T_N = 145$ K. These curves also give an indication of thermomagnetic irreversibility at 118 K, which along with the absence of inflection in specific heat results might be associated to spin-glass behavior. Results of AC susceptibility and magnetic hyperfine field measured using ¹¹¹In(¹¹¹Cd) probe nuclei carried out by perturbed angular correlations (PAC) technique did not show evidence of spin-glass behavior. The thermomagnetic irreversibility in FC-ZFC curves along with results of hyperfine interactions suggest the presence of magneto-crystalline anisotropy effects and a weak long-range coupling in GdMnIn.

© 2021 Author(s). All article content, except where otherwise noted, is licensed under a Creative Commons Attribution (CC BY) license (<http://creativecommons.org/licenses/by/4.0/>). <https://doi.org/10.1063/9.0000037>

I. INTRODUCTION

GdMn₂ is a member of a series of Laves phase compounds containing a rare-earth element and a magnetic 3d-transition metal with very peculiar magnetic properties, representing an interesting example of a frustrated 3D Mn sublattice where the competition between frustration, magnetic-nonmagnetic instability and anisotropy leads to complicated magnetic structures.^{1,2} The addition of a non-magnetic element such as indium results in the equiatomic GdMnIn compound affecting these properties and creating a detachment in the spin distribution that is a basic condition to spin glass behavior.^{3,4} This compound belongs to the ternary series RTX, where R is a rare-earth metal, T is a transition metal, and X is an sp element, which comprise intermetallic compounds showing interesting magnetic properties and a variety of magnetic structures.^{5,6} GdMnIn is reported to crystallize in the hexagonal MgNi₂, C14-Laves-type structure (space group $P6_3/mmm$) presenting a spin-glass behavior with no magnetic order attributed to the

triangular spin frustration of magnetic ions.⁴ In this crystalline network, Mn ions carry a substantial magnetic moment but magnetization, electrical resistivity and specific heat measurements have not shown signatures of long-range magnetic order, hindering the determination of the antiferromagnetic transition temperature with a certain degree of precision.

The spin-glass behavior in intermetallic systems is an interesting topic that opens theoretical questions as well as stimulates the use of different experimental techniques producing data to better understand these systems. Signatures of spin-glass behavior are the order-disorder lattice that induces spin fluctuations, geometric spin frustration, and competing ferromagnetic (FM) and antiferromagnetic (AFM) interactions.^{7,8} Spin Frustration can be found in systems where there is competition between magnetic interactions and the topology of the magnetic atoms. Good examples are the triangular Kagomé 2D lattice and the so-called pyrochlore lattice or base-to-base plane, apex-to-apex along c-axis (for the C14 structure) in 3D isotropic frustrated system.^{9–12}

In addition, intermetallic compounds containing rare-earth and transition metal elements with 4f- and 3d-electrons present a complex magnetism due to the interplay of exchange interactions between these electrons. On one hand, because the localized character of the 4f band, the interaction between 4f spins and the spin of itinerant electrons occurs locally through the exchange on the rare-earth ion and, therefore, its coupling with 4f spins of nearest neighboring rare-earth is indirect resulting in relative low ordering temperatures of the rare-earth sublattice.¹³ On the other hand, as the 3d band is broader, the exchange between the spins of 3d electrons in transition metals is direct with magnetic ordering at higher temperatures. Moreover, the nature of the magnetic exchange interactions between 3d and 4f ions is not well understood yet. Again, due to the localized character of 4f band the exchange interaction between 4f and 3d spins may be indirect and mediated by 5d electrons. A ferromagnetic coupling occurs between the 4f and the 5d electron spins whereas the 5d and 3d spins couple antiferromagnetically.^{14,15}

The observed absence of long-range interactions by magnetization measurements along with almost impossible measurements with neutron diffraction due to the presence of Gd with very high neutron absorption cross section makes the investigation of local exchange interactions in this compound very difficult. In the work reported here, measurements of hyperfine interactions at In sites were carried out to obtain information at atomic level especially to investigate the local magnetic exchange interactions in GdMnIn compound. ¹¹¹Cd, resulting from the decay of radioactive ¹¹¹In, was used as probe nuclei in the measurements with perturbed angular correlations (PAC) technique. This technique is highly sensitivity to the local magnetic interactions as well as electronic distribution around the probe nuclei. Additionally, magnetization measurements were also carried using a superconducting quantum interference device (SQUID) magnetometer. The temperature dependence of hyperfine parameters along with magnetization results formed a complete picture of the magnetic behavior as well as allowed the understanding the peculiar magnetism in this compound.

II. EXPERIMENTAL PROCEDURE

The GdMnIn samples were prepared by arc melting the constituent metals gadolinium (99.9%), manganese (99.999%) and indium (99.9999%) in stoichiometric proportions (with a 3 wt% excess of Mn to compensate the loss by evaporation during arc melting) under argon atmosphere. After melting, samples were sealed in an evacuated quartz tube and subjected to annealing at 600 °C for 12 h in order to reduce the strain of the crystal lattice. The crystal structure was checked by X-ray diffraction (XRD) in order to determine the structural parameters. Room temperature powder XRD pattern was recorded using a Cu-K α radiation with 2 θ ranging from 10° to 80° in step size of 0.05° and 5 s/step counting time in an automated Nicolet-Stoe diffractometer L11 at McGill University. In order to determine the structural parameters the standard Rietveld refinement by GSAS program was used. The magnetic characterization of the sample was performed using a superconducting quantum interference device (SQUID) magnetometer yielding the Zero-Field-Cooling (ZFC) and Field Cooling (FC) curves. To obtain the ZFC curve, the sample was first cooled in a zero field until low

temperature (2 K) and then a field of 100 Oe was applied until the temperature reached 300 K. After heating, the sample was cooled down again to the lowest temperature of 2 K with field applied obtaining the FC curve. For PAC measurements, the radioactive probe nuclei were introduced by re-melting the sample with the addition of a few drops (containing about 50 micro Curies) of carrier free ¹¹¹In solution. In the present work, ¹¹¹Cd, the daughter nucleus resulting from the electron-capture decay of the parent ¹¹¹In, hereafter represented as ¹¹¹In(¹¹¹Cd), was used as probe nucleus to measure the hyperfine interactions. The measurements were carried out in a spectrometer with four-BaF₂ detectors in the temperature range from 15 K to 295 K using a closed-cycle helium cryogenic system and from 300 K to 483 K using a small furnace.

PAC measurements yield gamma-gamma coincidence spectra between any two detectors forming angles of 90° or 180°. The ratio of the coincidence spectra gives the spin-rotation function $R(t) = A_{22} \sum_i f_i G_{22}^i(t)$, which is fitted by using a model that takes into account the fractional site population of probe nuclei f_i and its respective perturbation function $G_{22}^i(t)$. A_{22} is the angular correlation coefficient, which, for the gamma cascade in ¹¹¹In(¹¹¹Cd) equals -0.18.¹⁶ For magnetic hyperfine interactions, $G_{22}(t) = 0.2 + 0.4 \sum_{n=1,2} \cos(n\omega_L t)$ and from its experimental determination one can extract $\omega_L = \mu_N g B_{hf} / \hbar$, where μ_N is the nuclear magneton and g is the nuclear g -factor. Thus the magnetic hyperfine field, B_{hf} , may be determined. The perturbation function for electric quadrupole interactions is given by $G_{22}(t) = S_{20} + \sum_{n=1,2,3} S_{2n} \cos(\omega_n t)$. The tran-

sition frequencies ω_n , as well as S_{2n} and $g_n(\eta)$ coefficients, are known functions of the components of diagonalized EFG tensor, V_{kk} . Assuming $|V_{xx}| \leq |V_{yy}| \leq |V_{zz}|$, $\omega_n = eQg_n(\eta)V_{zz}/\hbar$, where eQ is the electric quadrupole moment of the probe nuclei and $\eta = (V_{xx} - V_{yy})/V_{zz}$ is the asymmetry parameter. The width of frequency distribution is parametrized with $\delta\omega$. For both quadrupole electric and dipole magnetic static interactions a Lorentz broadening is assumed.

Spectra taken with ¹¹¹In(¹¹¹Cd) probe recorded at temperatures above 175 K were fitted with a model considering two fractions with pure electric quadrupole interactions characterized by different hyperfine parameters, hereafter referred as f_1 (major fraction) and f_2 (minor fraction). These parameters correspond to probe nuclei in distinct local environments. At low temperatures ($T \leq 175$ K) spectra were fitted with combined electric quadrupole plus magnetic dipole interactions. The value of $Q = 0.641$ b determined by H. Haas *et al.*¹⁷ was taken in the calculation of V_{zz} . Further details on TDPAC technique and the experimental procedure may be found elsewhere.^{18–20}

III. RESULTS AND DISCUSSION

A. XRD results

The X-Ray Diffractogram and Rietveld refinement of XRD pattern are shown in Fig. 1. A well defined hexagonal MgNi₂-Laves type structure with the space group $P6_3/mmc$ can be seen from the Rietveld refinement analysis. The lattice parameters obtained from the analysis are displayed in Table I which also shows the elementary composition (in percentage) of the GdMnIn sample for the sake of comparison with sample reported in literature. Although

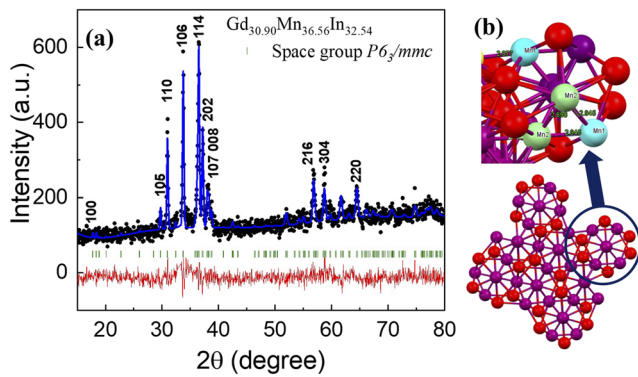


FIG. 1. (a) The Rietveld-refined powder XRD pattern at room temperature for $\text{Gd}_{30.90}\text{Mn}_{36.56}\text{In}_{32.54}$. The black circles, continuous blue line, continuous red line, and vertical green marks are corresponding data, refinement fit, difference, and theoretical Bragg peaks of $P6_3/mmc$, respectively. (b) Bottom, representative structure for GdMnIn with hexagonal MgNi_2 structure, C-14 type. Red spheres are Gd atoms and purple spheres are In and Mn atoms randomly distributed. Top, representative crystal structure in which the Mn ions occupy the corners of the tetrahedron. Blue, green, and yellow spheres represent Mn1, Mn2, and Mn3 atomic positions randomly occupied by Mn and In atoms.

TABLE I. Percentage composition and lattice parameters (a and c) obtained from Rietveld refinement analysis of measurement taken at room temperature on $\text{Gd}_{30.90}\text{Mn}_{36.56}\text{In}_{32.54}$ for $\text{Gd}(\text{Mn}_{1-x}\text{In}_x)_2$ phase with $P6_3/mmc$ space group and MgNi_2 -type structure.

Composition (at.%)	Lattice parameters (\AA)		References
	a	c	
$\text{Gd}_{33.3}\text{Mn}_{33.4}\text{In}_{33.3}$	5.786	18.817	Ref. 4
$\text{Gd}_{30.90}\text{Mn}_{36.56}\text{In}_{32.54}$	5.780	18.816	This Work

the results show a somewhat different elementary composition, the XRD refinement is consistent with $\text{Gd}_{33.3}\text{Mn}_{33.4}\text{In}_{33.3}$ compound as reported in previous work from De Negri *et al.*⁴ Schematic structure of hexagonal MgNi_2 , C-14 type structure for GdMnIn is also shown in Fig. 1. In this structure, Mn and In atoms are arranged randomly occupying sites 4f, 6g, 6h. However, it is important to note that our XRD pattern was fitted using the MgNi_2 type structure, in contrast to MgZn_2 type structure attributed in a previous report by Dar *et al.*³ However, De Negri *et al.*⁴ performed a careful and systematic analyses of $\text{Gd}(\text{Mn}_{1-x}\text{In}_x)_2$ compounds and noticed the similarity between the XRD patterns for MgZn_2 and the MgNi_2 type structures which can result in ambiguity in identifying the type of structure. The main difference between these two structures is the concentration of Mn which is approximately twice that of In in the case of the MgZn_2 -type structure in comparison with MgNi_2 -type structure which has comparable percentages for Mn and In atoms. Lattice parameters and elemental composition as well as atomic distances obtained in this study by GSAS refinement using Rietveld method are displayed in Tables I and II, respectively. Results are in good agreement with the data obtained by De Negri *et al.*⁴ for the equiatomic $\text{Gd}_{33.3}\text{Mn}_{33.4}\text{In}_{33.3}$ compound.

TABLE II. Distances in angstrom between atoms obtained from Rietveld refinement analysis of measurement taken at room temperature on $\text{Gd}_{30.90}\text{Mn}_{36.56}\text{In}_{32.54}$ for $\text{Gd}(\text{Mn}_{1-x}\text{In}_x)_2$ phase.

	This work	Ref. 4
$d_{\text{Gd}-\text{Gd}}$		
Gd1-Gd1	3.477(7)	3.477
Gd2-Gd2	3.549(8)	3.707
$d_{\text{Mn}-\text{Mn}}$		
Mn1-Mn2	2.945(5)	2.946
Mn1-Mn3	2.877(4)	2.878
Mn2-Mn2	2.890(5)	2.893
Mn3-Mn3	2.734(5)	2.737
$d_{\text{Gd}-\text{Mn}}$		
	$d_{\text{Gd1}-\text{Mn}}$	$d_{\text{Gd2}-\text{Mn}}$
Gd-Mn1	3.407(5)	3.374(5)
Gd-Mn2	3.373(5)	3.371(6)
Gd-Mn3	3.359(6)	3.392(5)

B. Magnetization results

Results of magnetic characterization of GdMnIn sample performed by using SQUID magnetometer are shown in Fig. 2(a) which displays the zero-field-cooled (ZFC) and field-cooled (FC) curves as well as the temperature dependence of the inverse of magnetic susceptibility. One can see from the curves an indication of thermomagnetic irreversibility of the ZFC-FC magnetization at $T_{\text{ir}} = 118$ K. This difference between the ZFC-FC curves in the equiatomic GdMnIn system is considered as a signature of the spin-glass behavior.²¹

Although the spin-glass assignment in this system may be a reasonable hypothesis based on this and other similar studies on the magnetic properties of canonical GdMn_2 Laves phases,^{1,2} since in this compound the magnetic contribution is due to the Mn atom, which form a tetrahedron that is present in either cubic (C15) or hexagonal (C14) environments. When the Mn atoms are randomly replaced by In atoms they produce a disorder in the system that might contribute to the spin-glass behavior. However, the thermomagnetic irreversibility of the ZFC-FC magnetization observed in the present study could also be attributed to the effects of magneto-crystalline anisotropy of the system.²²

The $M_{\text{ZFC-FC}}$ curves also exhibit an inflection which was ascribed to the antiferromagnetic transition at $T_N = 145$ K. A similar value of $T_N = 150$ K has been previously reported by Dhar *et al.*³ Additionally, at low temperatures, an steep increase starting around 40 K was observed in $M_{\text{ZFC-FC}}$ curves. This behavior is similar to what was reported for GdMn_2 , where a weak ferromagnetic coupling below 40 K was ascribed to the ordering of the Gd sublattice,^{1,23,24} since the Néel temperature of the Mn sublattice ($T_N = 100$ K) is much higher. The magnetic ordering of the rare-earth sub-lattice at lower temperatures in Mn-based compounds in which the Mn sub-lattice orders at higher temperatures governed by the Mn-Mn distance

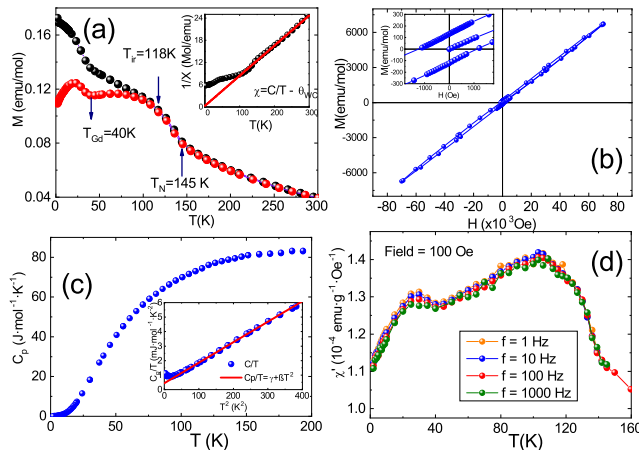


FIG. 2. (a) Temperature dependence of magnetization $M(T)$ curves for GdMnIn under zero-field-cooled (ZFC) and field-cooled (FC) at 100 Oe in the range from 5 K to 300 K. The inset shows the temperature dependence of the inverse of magnetic susceptibility fitted using Curie-Weiss law ($\chi = C/(T - \theta_{CW})$). (b) $M-H$ loop curve for GdMnIn measured at $T = 2$ K. (c) Temperature dependence of specific heat (C_p). The inset displays C_p/T vs. T^2 data below 40 K where open circles and red continuous line, respectively correspond to the experimental data and the linear fit. (d) Temperature dependence of AC magnetic susceptibility $\chi'(T)$ under different frequencies.

has also been observed in RMn_2Ge_2 ($R = \text{Pr, Nd}$).^{25–27} The inset in Fig. 2(a) displays the temperature dependence of the inverse magnetic susceptibility. Above 140 K, in a paramagnetic region, the curve was fitted by the Curie-Weiss law ($\chi = C/(T - \theta_{CW})$), where C is the Curie constant and θ_{CW} is the Weiss temperature. The small value of Weiss temperature ($\theta_{CW} = -3.8$ K) is an indication of the presence of weak antiferromagnetic interaction. From the fit of χ^{-1} (see inset in Fig. 2(a)), the C and θ_{CW} were calculated and we have used these values to determine the effective magnetic moment per formula unit given by $\mu_{eff} = 0.828 \times \sqrt{C \times MM} \mu_B$, where MM is the molecular mass of $\text{Gd}_{30.90}\text{Mn}_{36.56}\text{In}_{32.54}$ and the result is $\mu_{eff} = 9.92 \mu_B$.

We collected additional data in order to obtain the $M-H$ curve for the sample at low temperature (2 K) and high applied field displayed in Fig. 2(b). A clear absence of S-like shape without saturation was observed in the magnetization curve. However, as can be seen in the inset, a substantial coercivity ($H_c = 1200$ Oe) and a remanence ($M_r = 120$ emu/g) was determined. These findings are consistent with previously reported values where this behavior has been attributed to a spin-glass magnetism in this compound.^{3,4,22}

Fig. 2(c) also shows the temperature dependence of the specific heat $C_p(T)$ for GdMnIn in a temperature range from 5 K to 200 K. No inflexion around $T_N = 145$ K was observed in the $C_p(T)$ curve as temperature decreases. The absence of inflection thus confirms the absence of the long range magnetic order as observed by Dhar *et al.*³ As temperature further decreases, the value of C_p decreases smoothly till 2 K and no anomaly was observed. The inset of Fig. 2(c) shows the C_p/T versus T^2 plot below 40 K as well as the linear fit to the experimental curve according to the equation $C_p/T = \gamma + \beta T^2$.

As already mentioned, the irreversibility of $M_{ZFC-FC}(T)$ and $M(H)$ curves was considered as an indicator of the spin-glass behavior in GdMnIn as reported earlier.^{3,4} However, a finger print of spin-glass behavior can be observed by dynamic magnetic susceptibility technique, also called AC susceptibility (χ' and χ''), where the peak of susceptibility shifts in temperature with the variation of the frequency. In order to check the occurrence of any shift, we have measured the temperature dependence of the AC susceptibility for different frequencies $f = 1, 10, 100$ e 1000 Hz. The real parts of the AC magnetic susceptibilities χ' are shown in Fig. 2(d). Results show that χ' did not appreciably show any frequency dependence of the ordering temperature which rules out the possibility of presenting spin-glass nature. Hence this suggests that the bifurcation between ZFC and FC magnetization in GdMnIn could be completely ascribed to the existence of anisotropic magnetocrystalline effect.

C. PAC results

In order to obtain additional information on the exchange interactions in GdMnIn, we carried out measurements of hyperfine interactions at ^{111}In (^{111}Cd) probes located at In sites. The spin rotation spectra $R(t)$ taken at different temperatures (not displayed) show an evident change in patterns at low temperatures due to the magnetic ordering.

The results of the temperature dependence of the hyperfine parameters obtained from the fit to the experimental PAC spectra measured with ^{111}In (^{111}Cd) are shown in Fig. 3. The quadrupole interaction at major fraction f_1 was found to be axially symmetric ($\eta = 0$), whereas the asymmetry parameter for the minor fraction f_2 is temperature-dependent as displayed in Fig. 3. The figure also shows the electric field gradient tensor (V_{zz}) for site fraction f_1 and the temperature dependence of f_1 and f_2 . We have assigned f_1 to probe nuclei substituting regular In sites in GdMnIn structure, whereas f_2 probably corresponds to probe nuclei at defective In sites such as those with a high degree of disorder in its neighborhood or near the surface boundary of grains.

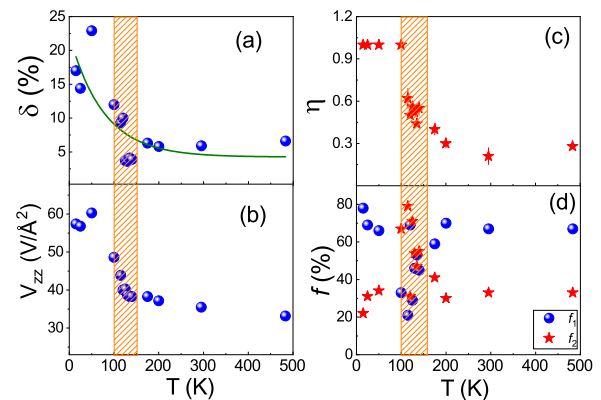


FIG. 3. Temperature dependence of (a) the distribution δ of (b) the major component f_1 of electric field gradient tensor V_{zz} , (c) the asymmetry parameter (η) for f_2 site, and (d) the fractional populations f_1 and f_2 measured in GdMnIn with ^{111}In (^{111}Cd) probe nuclei. Results for site f_1 are represented by blue spheres and those of site f_2 by red stars. The solid curve in (a) is the fit of an exponential function with the purpose to guide the eyes. Dashed region roughly shows the transition due to the presence of combined electric quadrupole plus magnetic dipole interactions.

At 483 K, well above the magnetic transition temperature, the hyperfine parameters for the major and the minor fractions are $V_{zz}^{(1)} = 33.2(1) \text{ V}/\text{\AA}^2$, $\delta^{(1)} \sim 6\%$, $\eta^{(1)} = 0$, $f_1 = 67\%$, and $V_{zz}^{(2)} = 38.0(2) \text{ V}/\text{\AA}^2$, $\eta^{(2)} = 0.28$, $\delta^{(2)} \sim 24\%$, $f_2 = 33\%$ respectively.

Specific heat results do not indicate any change at low temperatures weakening the association of the kink in M_{ZFC-FC} curves at 40 K with a possible structural transition. On the other hand, results of electric field gradient, a very local and sensitive parameter, show an increase in V_{zz} when temperature decreases below around 140 K, which would indicate a local structural change. However, the quadrupole frequency distribution increases significantly below the same temperature (see Fig. 3a) which is a strong evidence for atomic displacements or chemical disorder. Results of magnetic hyperfine interactions can help to identify the observed transition at 40 K.

The magnetic hyperfine field (B_{hf}) and the angle (β) between the directions of V_{zz} and B_{hf} as a function of temperature are shown in Fig. 4. The magnetic ordering temperature determined from the figure is around $T_N = 145 \text{ K}$, in excellent agreement with the magnetization results. There is also a clear increase in B_{hf} values below around 40 K, which can be ascribed to the ordering of Gd sub-lattice reinforcing the observation with magnetization measurements as shown in Fig. 2(a). The temperature dependence of the angle β shows a strong variation just below the magnetic transition temperature within a range from $\sim 120 \text{ K}$ to $\sim 140 \text{ K}$, but below 100 K it increases smoothly up to 130° .

The change in the angle can be attributed either to a change in the direction of V_{zz} or the direction of B_{hf} . The value of V_{zz} increases when the temperature decreases (see Fig. 3). A change in the value and direction of V_{zz} certainly would affect the other components, V_{xx} and V_{yy} , causing a change in the asymmetry parameter η , which is not observed. Therefore, we assume that the direction of B_{hf} changes when the temperature decreases, probably influenced by the ordering of Gd sub-lattice. In the temperature range from 175 K to 483 K, V_{zz} decreases almost linearly with temperature. The value

of V_{zz} at 300 K is very similar to that reported previously for GdMn_2 with PAC measurements using ^{111}Cd probe nuclei.^{28,29} At 15 K we observed a pronounced increase in the value of V_{zz} . This increase is surely related with the magnetic ordering and possibly the effect of Gd sub-lattice ordering.

The value of B_{hf} extrapolated to zero kelvin is around 1.1 T, which is far below the value also extrapolated to zero Kelvin of $B_{hf} = 7 \text{ T}$ for the GdMn_2 compound²⁸ also measured with $^{111}\text{In}(^{111}\text{Cd})$ at Mn sites. $B_{hf} = 4 \text{ T}$ at $T = 0 \text{ K}$ was reported for ^{119}Sn at Mn sites in GdMn_2 measured with Mössbauer spectroscopy.¹ As both Cd and Sn are diamagnetic with closed 3d shell, the lower value of B_{hf} for ^{119}Sn results can be ascribed to the concentration of Sn (around 0.2 at%) a value much higher than around 0.1 ppm of $^{111}\text{In}(^{111}\text{Cd})$. This effect is much intense in GdMnIn where half of Mn atoms are replaced by In and it is confirmed by our results with $B_{hf} = 1.1 \text{ T}$ at 0 K. On the other hand, the magnetic hyperfine field measured with $^{111}\text{In}(^{111}\text{Cd})$ was reported to be 10 T and 12 T, respectively, in GdPdIn^{30} and GdNiIn^{31} . Although these compounds have a quite similar stoichiometry as GdMnIn , their magnetic properties are different with the magnetic moment localized only in Gd atoms that order ferromagnetically. Considering only the magnetic hyperfine field from Mn sublattice in GdMn_2 , estimated to be around 2 T from measurements with ^{119}Sn at 80 K,¹ $B_{hf} = 6.7 \text{ T}$ measured with $^{111}\text{In}(^{111}\text{Cd})$ in metallic Mn,³² and our result at 100 K, $B_{hf} = 0.7 \text{ T}$, we observe that these values are almost proportional to the quantity of Mn atoms per formula unit, which is respectively are 2/3, 3/3, and 1/3. The exchange mechanism is, therefore, similar in these compounds, where a magnetic coupling of Mn atoms is present. Moreover, a local signature of spin-glass behavior observed through magnetic hyperfine field is its high degree of distribution,³³ which is not verified in this work (see Fig. 3). The observed change in the direction of B_{hf} relative to V_{zz} can be an indication of an anisotropy effect on the magnetic ordering.

IV. SUMMARY

Magnetic properties of GdMnIn intermetallic compound with Laves-phase-type structure has been investigated through measurements of hyperfine interactions by PAC using $^{111}\text{In}(^{111}\text{Cd})$ as probe nuclei as well as bulk magnetization measurements. Although ZFC-FC magnetization curves and the temperature dependence of the specific heat measurements indicate a possible spin-glass behavior, AC susceptibility (at high frequencies) and PAC measurements at In sites did not show dynamic dependence, which evidences a spin-glass behavior. This discrepancy can be attributed to a chemical disorder due to the In substitution leading to a magneto-crystalline anisotropy, possibly also observed by local measurements. Moreover, a clear increase in the ZFC curve below 40 K indicates a long-range coupling of Gd sublattice, which is also observed in the temperature dependence of B_{hf} . We, therefore, rule out the presence of spin-glass behavior in GdMnIn and conclude that a weak long-range coupling is present below the ordering temperature.

ACKNOWLEDGMENTS

Partial financial support for this work was provided by Fundação de Amparo a Pesquisa do Estado de São Paulo (FAPESP) under grant 2014/140001-1. AWC and RNS acknowledge the

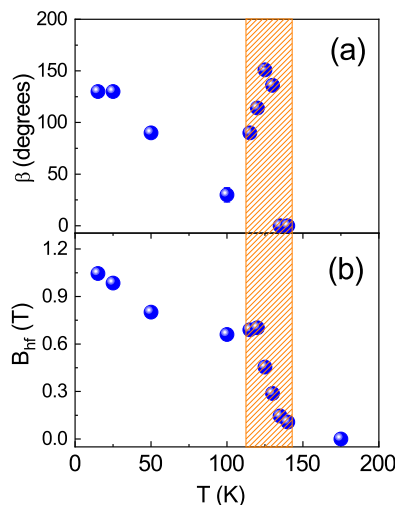


FIG. 4. Temperature dependence of (a) the angle β , and (b) the magnetic hyperfine field (B_{hf}) measured with $^{111}\text{In}(^{111}\text{Cd})$ in GdMnIn .

Conselho Nacional de Desenvolvimento Científico e Tecnológico (CNPq) for financial support in a form of research fellowship (grant 304627/2017-8). AB greatly acknowledges the financial support of FAPESP (grant 2019/15620-0). Finally, GACP kindly acknowledges the Department of Physics of McGill University where the XRD measurements were carried out.

DATA AVAILABILITY

The data that support the findings of this study are available from the corresponding author upon reasonable request.

REFERENCES

- ¹K. Krop, *Physica B* **319**, 9–16 (2002).
- ²E. Talik, M. Neumann, T. Mydlarz, J. Kusz, H. Böhm, A. Winiarski, and A. Gilewski, *J. Phys.: Condens. Matter* **10**, 581–592 (1998).
- ³S. K. Dhar, C. Mitra, P. Manfrinetti, R. Palenzona, and A. Palenzona, *J. Phase Equilibria* **23**, 79–82 (2002).
- ⁴S. D. Negri, D. Kaczorowski, A. Grytsiv, E. Alleno, M. Giovannini, R. Gorzelniak, P. Rogl, C. Godart, A. Saccone, and R. Ferro, *J. Alloys Compounds* **365**, 58–67 (2004).
- ⁵A. Szytula and J. Leciejewicz, *Handbook of Crystal Structures and Magnetic Properties of Rare Earth Intermetallics* (CRC, 1994).
- ⁶G. Ehlers and H. Maletta, *Physica B* **234–236**, 667 (1997).
- ⁷J. A. Midosh, *J. Magn. Magn. Mater.* **157–158**, 606–510 (1996).
- ⁸J. A. Midosh, *Spin Glasses: An Experimental Introduction* (Taylor and Francis, 1993).
- ⁹S. T. Bramwell and M. J. P. Gingras, *Science* **294**, 1495–1501 (2001).
- ¹⁰K. Matsuhira, Z. Hiroi, T. Tayama, S. Takagi, and T. Sakakibara, *J. Phys.: Condens. Matter* **14**, L559–L565 (2002).
- ¹¹A. J. MacDonald, P. C. W. Holdsworth, and R. G. Melko, *J. Phys.: Condens. Matter* **23**, 164208 (2011).
- ¹²A. S. Wills, R. Ballou, and C. Lacroix, *Phys. Rev. B* **66**, 144407 (2002).
- ¹³H.-S. Li, Y. P. Li, and J. M. D. Coey, *J. Phys.: Condens. Matter* **3**, 7277–7290 (1991).
- ¹⁴I. A. Campbell, *J. Phys.F: Metal Phys.* **2**, L47 (1972).
- ¹⁵M. S. S. Brooks, O. Eriksson, and B. Johansson, *J. Phys.:Condens. Matter* **1**, 5861–5874 (1989).
- ¹⁶H. H. Rinneberg, *At. Energy Rev.* **17**, 477–595 (1979).
- ¹⁷H. Haas, S. P. A. Sauer, L. Hemmingsen, V. Kellö, and P. W. Zhao, *Eur. Phys. Lett.* **117**, 62001 (2017).
- ¹⁸M. O. Zacate and H. Jaeger, *Defect and Diffusion Forum* **311**, 3 (2011).
- ¹⁹A. W. Carbonari, J. Mestnik-Filho, and R. N. Saxena, *Defect and Diffusion Forum* **311**, 39 (2011).
- ²⁰G. Schatz and A. Weidinger, *Nuclear Condensed Matter Physics: Nuclear Methods and Applications* (Wiley, 1996).
- ²¹C. S. Lue, Y. Oner, D. G. Naugle, and J. J. H. Ross, *Phys. Rev. B* **63**, 184405 (2001).
- ²²P. Manfrinetti, A. Palenzona, S. K. Dhar, C. Mitra, P. L. Paulose, D. Pal, and S. Ramakrishnan, *J. Magn. Magn. Mater.* **213**, 404–412 (2000).
- ²³S. K. Malik and W. E. Wallace, *J. Magn. Magn. Mater.* **24**, 23–28 (1981).
- ²⁴J. Przewoznik, J. Zukrowski, and K. Krop, *J. Magn. Magn. Mater.* **119**, 150–160 (1993).
- ²⁵B. Bosch-Santos, A. W. Carbonari, G. A. Cabrera-Pasca, R. N. Saxena, and R. S. Freitas, *J. Appl. Phys.* **117**, 17E304 (2015).
- ²⁶B. Bosch-Santos, G. A. Cabrera-Pasca, R. N. Saxena, R. S. Freitas, and A. W. Carbonari, *AIP Adv* **7**, 056211 (2017).
- ²⁷B. Bosch-Santos, G. A. Cabrera-Pasca, R. N. Saxena, A. N. Burimova, and A. W. Carbonari, *Physica B* **536**, 137–141 (2018).
- ²⁸A. A. Tulapurkar and S. N. Mishra, *Hyperf. Interact.* **120/121**, 247–251 (1999).
- ²⁹M. F. S. C. Bedi and H. Euler, *Phys. Rev. B* **78**, 104202 (2008).
- ³⁰A. L. Lapolli, A. W. Carbonari, J. Mestnik-Filho, D. M. T. Leite, and R. N. Saxena, *Hyperf. Interact.* **176**, 75–79 (2007).
- ³¹A. L. Lapolli, R. N. Saxena, J. Mestnik-Filho, D. M. T. Leite, and A. W. Carbonari, *J. Appl. Phys.* **101**, 09D510 (2007).
- ³²G. D. Doncker, J. V. Cauteren, E. Tieghem, and M. Rots, *Phys. Rev. B* **39**, 12069–12077 (1989).
- ³³M. Rots, L. Hermans, and J. Van Cauteren, *Phys. Rev. B* **30**, 3666–3671 (1984).